REPORT

SOLID-STATE PHYSICS

Pascal conductance series in ballistic one-dimensional LaAlO₃/SrTiO₃ channels

Megan Briggeman^{1,2}*, Michelle Tomczyk^{1,2}, Binbin Tian^{1,2}, Hyungwoo Lee³, Jung-Woo Lee³, Yuchi He^{2,4}, Anthony Tylan-Tyler^{1,2}, Mengchen Huang^{1,2}, Chang-Beom Eom³, David Pekker^{1,2}, Roger S. K. Mong^{1,2}, Patrick Irvin^{1,2}, Jeremy Levy^{1,2}*

One-dimensional electronic systems can support exotic collective phases because of the enhanced role of electron correlations. We describe the experimental observation of a series of quantized conductance steps within strongly interacting electron waveguides formed at the lanthanum aluminate–strontium titanate (LaAlO₃/SrTiO₃) interface. The waveguide conductance follows a characteristic sequence within Pascal's triangle: $(1, 3, 6, 10, 15, ...) \cdot e^2/h$, where e is the electron charge and h is the Planck constant. This behavior is consistent with the existence of a family of degenerate quantum liquids formed from bound states of n = 2, 3, 4, ... electrons. Our experimental setup could provide a setting for solid-state analogs of a wide range of composite fermionic phases.

n one-dimensional (1D) systems of interacting fermions (1-4), correlations are enhanced relative to higher dimensions. A variety of theoretical approaches have been developed for understanding strongly correlated 1D systems, including Bethe ansatz and density matrix renormalization group (DMRG) (5). Experimentally, degenerate 1D gases of paired fermions have been explored in ultracold atom systems with attractive interactions (6). In the solid state, attractive interactions have been engineered in carbon nanotubes by means of a proximal excitonic pairing mechanism (7). Electron pairing without superconductivity, indicating strong attractive interactions, has been reported in low-dimensional SrTiO₃ nanostructures (8, 9). However, bound states of three or more particles-analogs of baryon phases (10)—have been observed only in few-body bosonic systems (11).

SrTiO₃-based electron waveguides can provide insight into strongly interacting fermionic systems. The total conductance through an electron waveguide is determined by the number of extended subbands (indexed by orbital, spin, and valley degrees of freedom) available at a given chemical potential μ (12, 13). Each subband contributes one quantum of conductance e^2/h with transmission probability $T(\mu)$ to the total conductance $G = (e^2/h)\sum_i T_i(\mu)$ (14). Quantized transport was first observed in III-V quantum point contacts (15, 16) and subsequently in 1D systems (17–19). Quantized con-

in table S1. The conductance of these electron waveguides depends principally on the chemical potential u and the applied external magnetic field **B** (Fig. 1A). The chemical potential is adjusted with a local side gate $V_{\rm sg}$ (9); for most experiments described here, the external magnetic field is oriented perpendicular to the LaAlO₃/SrTiO₃ interface: $\mathbf{B} = B_z \hat{z}$. Quantum point contacts formed in semiconductor heterostructures (15, 16) exhibit conductance steps that typically follow a linear sequence: $2 \times$ $(1, 2, 3, 4, ...) \cdot e^2/h$, where the factor of 2 reflects the spin degeneracy. In an applied magnetic field, the electronic states are Zeeman-split, and they resolve into steps of $(1, 2, 3, 4, ...) \cdot e^2/h$. In contrast, here we find that for certain values of magnetic field, the conductance steps

duction within 1D electron waveguides was

recently demonstrated within LaAlO₃/SrTiO₃

heterostructures (9). A unique aspect of this

SrTiO₃-based system is the existence of tunable

electron-electron interactions (20) that lead

to electron pairing and superconductivity (8).

Here, we investigated LaAlO₃/SrTiO₃-based 1D

electron waveguides that are known to exhibit

quantized ballistic transport as well as sig-

natures of strong attractive electron-electron

interactions and superconductivity (8, 9, 20).

Fabrication details are described in (21). More

than a dozen specific devices have been investigated. Parameters and properties for seven

representative devices (devices 1 to 7) are given

In order to better understand the origin of this sequence, it is helpful to examine the transconductance $dG/d\mu$ and plot it as an intensity

for LaAlO₃/SrTiO₃ electron waveguides follow the sequence $(1, 3, 6, 10, ...) \cdot e^2/h$, or $G_n = n(n + 1)$

 $1)/2 \cdot e^2/h$. As shown in Fig. 1B, this sequence of

numbers is proportional to the third diagonal

of Pascal's triangle (Fig. 1C, highlighted in red).

map as a function of B and μ . Transconductance maps for devices 1 to 6 are plotted in Fig. 2. A peak in the transconductance demarcates the chemical potential at which a new subband emerges; these chemical potentials occur at the minima of each subband, and we refer to them as subband bottoms (SBBs). The peaks generally shift upward as the magnitude of the magnetic field is increased, sometimes bunching up and then again spreading apart. We observe many of the same features that were previously reported in 1D electron waveguides in LaAlO₃/SrTiO₃ (9), such as electron pairing and re-entrant pairing, which indicate the existence of electron-electron interactions. Near a special value of the magnetic field, multiple subbands lock, and the total conductance as a function of chemical potential follows a Pascal series that is quantized in units of e^2/h (see the labeled conductance plateaus in Fig. 2A).

Our approach to understanding the transport results described above begins with a single-particle description and incorporates interactions when the original description breaks down. Outside of the locked regions, the system is well described by a set of non-interacting channels, which places strong constraints on the theory of the locked regions. Any theory of the locked phases would need to explain the locking of the transconductance peaks as well as quantized conductance steps away from the locked regime.

Our single-particle description excludes interactions but takes into account the geometry of the electron waveguide that produces the underlying subband structure. The singleparticle picture has four components: confinement of electrons in the (i) vertical and (ii) lateral directions by the waveguide, and an external magnetic field that affects the electrons via the (iii) Zeeman and (iv) orbital effects. The intersection of more than two SBBs requires a special condition to be satisfied in the singleparticle model. The degeneracy requirement for obtaining the Pascal series (i.e., the crossing of 1, 2, 3, 4, ... SBBs) is satisfied by a pair of ladders of equispaced levels. Indeed, a pair of ladders of equispaced levels is naturally produced by a waveguide with harmonic confinement in both vertical and lateral directions. In the presence of Zeeman interactions, the waveguide Hamiltonian can be written as

$$H = rac{(p_x - eB_z y)^2}{2m_x^*} + rac{p_y^2}{2m_y^*} + rac{p_z^2}{2m_z^*} + rac{m_y^* \omega_y^2}{2} y^2 + rac{m_z^* \omega_z^2}{2} z^2 - g \mu_{
m B} B_z s \qquad (1)$$

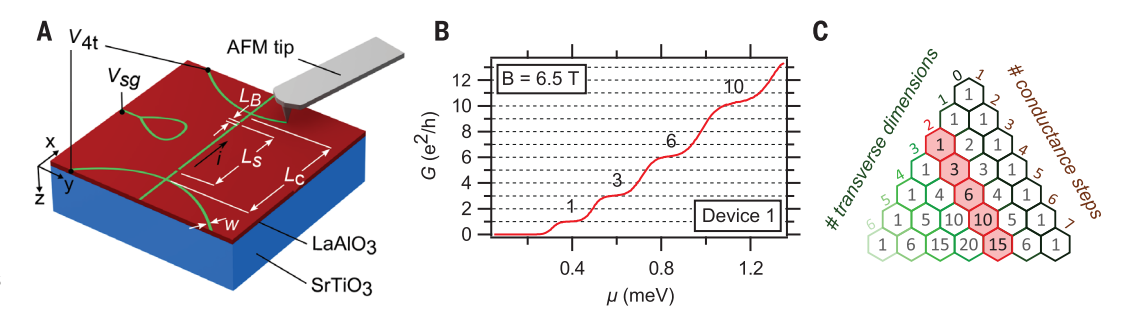
(9), where m_x^* , m_y^* , and m_z^* are the effective masses along the x, y, and z directions; ω_y and ω_z are frequencies associated with parabolic transverse confinement in the lateral (y) direction and half-parabolic confinement in the vertical (z > 0) direction, respectively; g is the

megan.briggeman@levylab.org (M.B.)

¹Department of Physics and Astronomy, University of Pittsburgh, Pittsburgh, PA 15260, USA. ²Pittsburgh Quantum Institute, Pittsburgh, PA 15260, USA. ³Department of Materials Science and Engineering, University of Wisconsin, Madison, WI 53706, USA. ⁴Department of Physics, Carnegie Mellon University, Pittsburgh, PA 15213, USA. *Corresponding author. Email: jlevy@pitt.edu (J.L.);

Fig. 1. Pascal series of conduction steps in an electron

waveguide. (A) Depiction of the sketched waveguide. Green lines indicate conductive paths at the LaAlO₃/SrTiO₃ interface. Device dimensions are indicated: barrier width $L_{\rm B}$, barrier separation $L_{\rm S}$, total length of the channel between the voltage sensing leads $L_{\rm C}$, and nanowire width as measured at room temperature,



typically $w \sim 10$ nm. A current i through the waveguide produces a voltage V_{4t} , corresponding to a conductance $G = di/dV_{4t}$. (B) Conductance $G = di/dV_{4t}$. (C) Pascal triangle representation of observed conductance steps, represented in units of e^2/h . The highlighted diagonal represents the sequence for an electron waveguide with two transverse degrees of freedom.

Landé factor; μ_B is the Bohr magneton; and $s=\pm \frac{1}{2}$ is the spin quantum number. Eigenenergies corresponding to the SBBs are given by

$$egin{align} E_{n_z,n_y,s} &= \hbar\Omegaigg(n_y+rac{1}{2}igg) + \ \hbar\omega_zigg[(2n_z+1)+rac{1}{2}igg] - g\mu_{
m B}B_z s \ \end{align}$$

where the electron eigenstates $|n_z, n_w, s\rangle$ are indexed by the orbital quantum numbers n_z and n_y and spin quantum number s, \hbar is the Planck constant divided by 2π , and $\Omega = \sqrt{\omega_y^2 + \omega_c^2}$ is the magnetic field-dependent frequency associated with parabolic confinement of the electron in the lateral direction (calculated from the bare frequency ω_{ν} and the cyclotron frequency $\omega_{\rm c}=eB_z/\sqrt{m_x^*m_y^*}$). To obtain two equispaced ladders of states, we use the states associated with Ω for the first ladder and the states associated with ω₂₂ split by the Zeeman splitting, for the second ladder. The Pascal series is produced by the "Pascal condition": $\Omega = 4\omega_z = 2g\mu_B B_z/\hbar$. This condition requires fine-tuning of both the magnetic field B_z and the geometry of the waveguide (ω_u/ω_z) . Meeting this condition results in crossings of increasing numbers of SBBs at a unique Pascal field B_{Pa} . By fitting the SBB energies given by Eq. 2 to experimental data, we are able to generate a peak structure (Fig. 3A) that is in general agreement with and has the same sequence of peak crossings as the experimentally observed transconductance. (Estimates for the single-particle model parameters are listed in table S1.) By intentionally detuning the parameters away from the Pascal condition (e.g., Fig. 3B), the SBBs no longer intersect at a well-defined magnetic field. Fits of the single-particle model to experimental data for devices 1 to 7 (Fig. 3C) show the expected correlation between ω_z and $\Omega(B_{\rm Pa})$, but we do observe deviations from the Pascal condition for all samples.

The experimental data deviate from the single-particle model in several important ways. At low magnetic fields, the predicted linear

Zeeman splitting of subbands is not obeyed; instead, the two lowest subbands ($|0, 0, \pm \frac{1}{2}\rangle$) are paired below a critical magnetic field, B_P (9). At higher magnetic fields, re-entrant pairing is observed as subbands intersect and lock over a range of magnetic field values near the Pascal field, $B_{\rm Pa}$. In our noninteracting model (Eq. 1), there is a unique Pascal field B_{Pa} ; however, experimentally we find that the value of the Pascal field depends on the degeneracy $n: B_{\mathrm{Pa}}^{(n+1)} < B_{\mathrm{Pa}}^{(n)}$. This shift of B_{Pa} with the degeneracy may be caused by an anharmonic component to the confinement. Adding an anharmonic term to the single-particle model produces similar shifts of B_{Pa} (21). Table S1 shows the pairing field $B_{\rm P}$ and Pascal field $B_{\rm Pa}^{(2)}$ for devices 1 to 7. Devices with similar geometries display a variety of pairing fields and Pascal fields. This is not unexpected, given a previous study (8) in which the pairing field was found to vary from device to device and could be as large as $B_P = 11$ T. The cause for the differing strength of the pairing field is unknown but likely plays a role in the differing strengths of the locking for the Pascal degeneracies in this work. Fits of the transconductance data were made for the n = 2 and n = 3 peaks (or plateaus), and we found that the states are, in fact, locking together over a finite range of magnetic fields (fig. S1) (21). The Pascal series of conductance steps is observed for a variety of devices written with both short (50 nm) and long (1000 nm) electron waveguides, and at different angles ϕ with respect to the (100) crystallographic axis of the sample (angles are listed in table S1). Devices with wires written at angles of 0°, 45°, or 90° show no discernable difference.

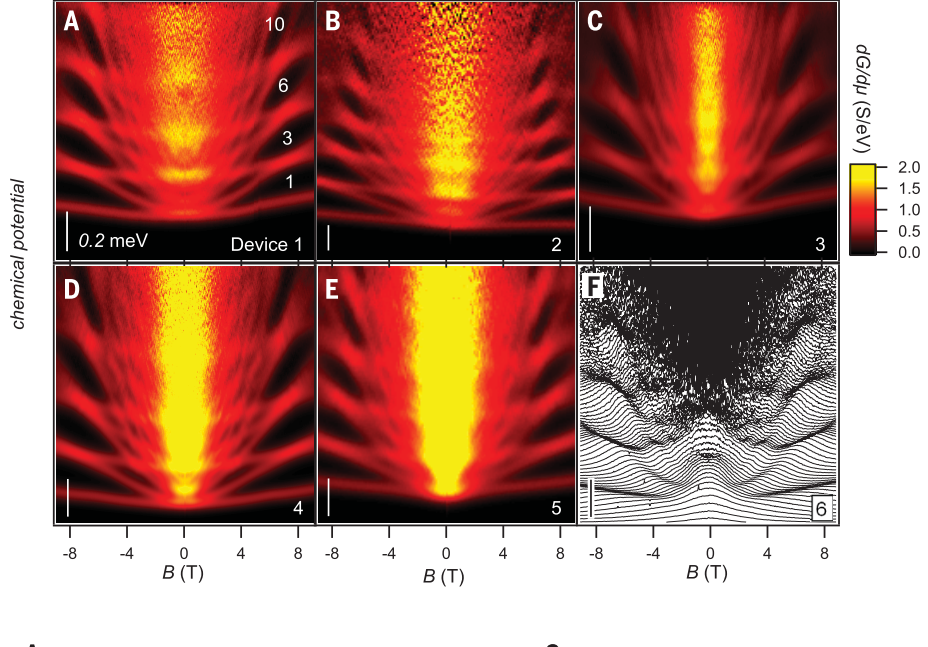
The Pascal condition assumes that the magnetic field is oriented out of plane. To investigate the effect of in-plane magnetic field components on the Pascal conductance series, we measure angle-dependent magnetotransport, with the magnetic field oriented at an angle θ with respect to the sample normal, within the *y-z* plane, $\mathbf{B} = B(\sin\theta~\hat{y} + \cos\theta~\hat{z})$ (Fig. 4A). In the out-of-plane orientation ($\theta = 0^{\circ}$),

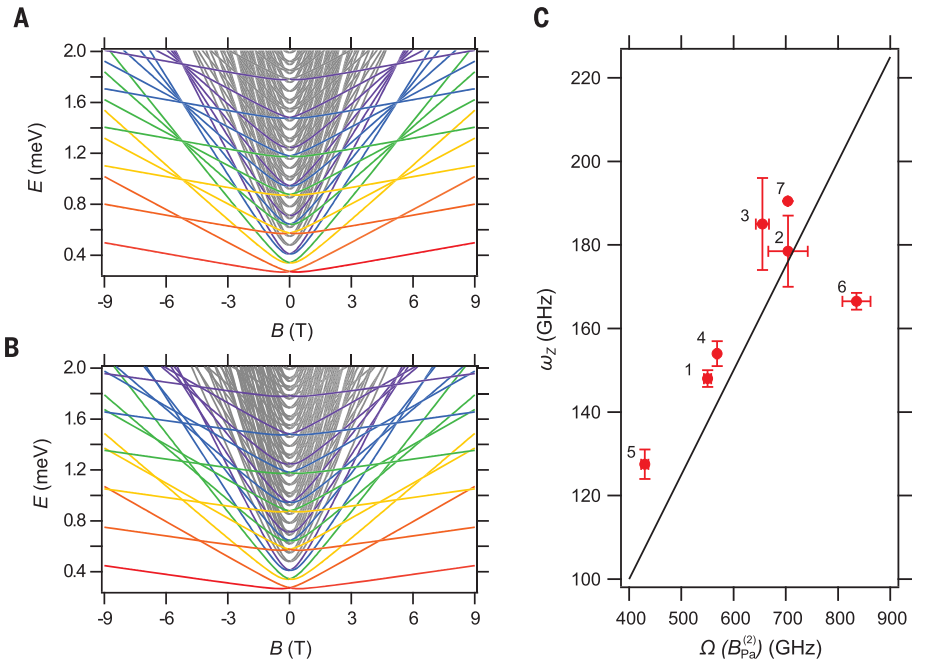
characteristic Pascal behavior is observed, with subband locking taking place near 6 T (Fig. 4D, $\theta = 0^{\circ}$). As θ increases, the subband locking associated with the n = 3 plateau destabilizes, while another (non-Pascal series) subband locking forms in a different region of parameter space (Fig. 4D, $\theta = 20^{\circ}$, indicated by white lines). At larger angles (Fig. 4D, $\theta = 50^{\circ}$), a dense network of re-entrant pairing, disbanding, and re-pairing is observed (movie S1). The strength of the re-entrant pairing of the $|0,0,\downarrow\rangle$ and $|0,1,\uparrow\rangle$ subbands is strongly dependent on the angle θ of the applied magnetic field (Fig. 4C). The lower (B_R^-) and upper (B_R^+) magnetic fields over which these SBBs are locked together are indicated by red and blue circles in Fig. 4D. The magnetic field range ($\Delta B_R = B_R^+ - B_R^-$) is shown as a function of angle (Fig. 4C). The strength of the re-entrant pairing, ΔB_R , initially increases with angle, jumps discontinuously at $\theta = 30^{\circ}$ as the SBBs (which have been shifting closer) snap together, and then decreases again. At $\theta = 0^{\circ}$, there is a non-Pascal series crossing (no locking) of like-spin states $(|0,0,\downarrow\rangle,|0,1,\downarrow\rangle)$, highlighted by crossed lines, which evolves into an avoided crossing at θ = 10°. This feature is explored in Fig. 4B, where we plot conductance curves at B = 3 T for different angles.

A theoretical analysis more sophisticated than the single-particle model discussed above is required to capture the effects of electronelectron interactions. In the absence of interactions, the single-particle model described by Eq. 1 has band crossings but cannot predict any locking behavior. Prior work has demonstrated the existence of attractive electron-electron interactions in LaAlO₃/SrTiO₃ nanostructures (8, 20). We therefore constructed an effective lattice model for the waveguide by extending the noninteracting model to include phenomenological, local, two-body interactions between electrons in different modes. This effective model was investigated using DMRG, a numerical method that produces highly accurate results for strongly interacting systems in one dimension (5, 22-27). The DMRG phase

Fig. 2. Transconductance maps of Pascal devices. (A to F) Transconductance dG/dµ plotted as a function of chemical potential μ and out-of-plane magnetic field B for representative devices 1 to 6, respectively. Bright regions indicate increasing conductance as new subbands become occupied; dark regions indicate conductance plateaus. Conductance values for several plateaus are indicated in white in (A), highlighting the Pascal series seen in all six devices shown here. Vertical scale bars in each panel represent 0.2 meV in chemical potential. The transconductance of device 6 is displayed as a waterfall plot with vertical offsets given by the chemical potential at which the curve was acquired. T = 50 mK.

Fig. 3. Subband energies for noninteracting electron waveguide model. (A) Energy E versus B calculated from the single-particle model, with parameters tuned to give Pascal degeneracies: $I_v = 33$ nm, $I_z = 10$ nm, $m_v = 1m_e$, $m_z = 5m_e$, g = 1.0. States are colored to highlight the bunching of increasing numbers of states to form the Pascal series conductance steps. (B) E versus B calculated from the single-particle model, where the parameters are the same as in (A), except that g = 1.2. (**C**) Plot of ω_z versus $\Omega(B_{Pa}^{(2)})$ for devices 1 to 7, showing that although ω_z and $\Omega(B_{Pa}^{(2)})$ vary from sample to sample, they are all near the theoretically predicted critical relationship $\omega_z = 0.25/[\Omega(B_{\rm Pa})]$, denoted by the solid black line.





diagrams in the vicinity of the n=2 and n=3 plateaus are shown in fig. S3. The first set of calculations reveal a phase boundary line between a vacuum phase and an electron pair phase that is characterized by a gap to single-electron excitations. We associate this line to the n=2 conductance step $(G=3e^2/h)$. Extending this calculation to three electron modes with attractive interactions (n=3 plateau) reveals a transition line from the vacuum phase to a "trion phase," which we associate with the n=3 conductance step $(G=6e^2/h)$. The trion phase is a 1D degenerate quantum liquid of composite fermions, each made up of three electrons, in which all one- and two-

particle excitations are gapped out but threeparticle excitations are gapless. [See (21) for details of our theoretical model and DMRG calculations.]

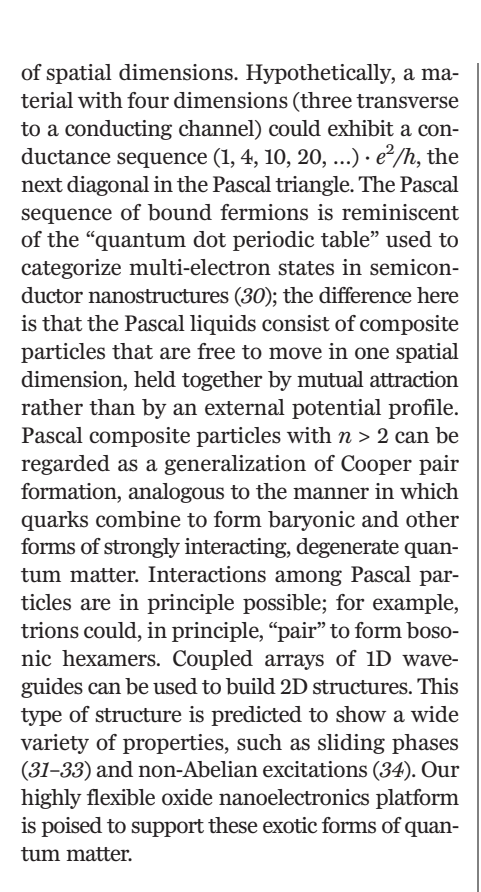
We considered other theoretical explanations. The addition of spin-orbit coupling to the noninteracting model modifies the subband structure, producing avoided crossings of the transconductance peaks. Anharmonicity of the confining potential, in the absence of interactions, bends the subband structure but also does not produce locking. We rule out impurity scattering effects because of the ballistic nature of the transport. Moreover, without inter-electron interactions [e.g., negative U

center (28)], an impurity cannot produce locking phenomena. We are not aware of other mechanisms for locking but cannot rule them out. Finally, we note that any theory of the locking phenomenon would need to have a noninteracting limit that matches with experiments (e.g., predicts conductance quantization).

Pascal composite particles predicted by our model would have a charge ne, where n=2,3,4,..., and spin quantum numbers not yet determined. As with fractional fermionic states, it seems likely that the expected charge could be verified from a shot-noise experiment (29). The particular Pascal sequence observed here experimentally is a consequence of the number

Fig. 4. Angle dependence of waveguide transport.

Data are from waveguide device 7. (A) Schematic of the sample as it is rotated with respect to the direction of the magnetic field **B**. \hat{n} is the vector normal to the plane of the sample, and $\theta = 0^{\circ}$ represents an out-of-plane magnetic field orientation. (B) Conductance curves as a function of angle at |B| = 3 T. As the magnetic field is rotated away from an out-of-plane angle, we see an avoided crossing open up, which can be seen in the $\theta = 10^{\circ}$ curve as the plateau that begins to form near $3e^2/h$. We can also see evidence that re-entrant pairing starts to occur at larger angles ($\theta > 30^{\circ}$) when the conductance increases by a step of $2e^2/h$, from $1e^2/h$ to $3e^2/h$. (C) Re-entrant pairing strength as a function of angle θ . (**D**) Transconductance $dG/d\mu$ as a function of magnetic field strength and chemical potential. The magnetic field is rotated from an outof-plane orientation ($\theta = 0^{\circ}$) to $\theta = 50^{\circ}$ in 10° steps. The in-plane component of the magnetic field is roughly perpendicular to the waveguide channel. At small angles, the Pascal series can be seen in the transport with bunches of 1, 2, and 3 subbands, but this is broken as the angle is increased. The reentrant pairing strength is indicated by the points where the states first lock together (red circles) and break apart (blue circles). T = 20 mK.



REFERENCES AND NOTES

- S. Tomonaga, Prog. Theor. Phys. 5, 544-569 (1950).
- 2. J. M. Luttinger, J. Math. Phys. 4, 1154-1162 (1963).

3. T. Giamarchi, Quantum Physics in One Dimension (Oxford Univ.

8

B (T)

- D. C. Mattis, E. H. Lieb, J. Math. Phys. 6, 304-312 (1965).
- S. R. White, Phys. Rev. Lett. 69, 2863-2866 (1992).

В

 (e^2/h)

1.2

1.0

8.0

0.6

0.4

0.2

0.0

1.4

1.2

1.0

0.8

0.6

0.4

0.2

Press, 2003).

0

|B| = 3 T

0.2 0.4 0.6 0.8

 $\theta = 0^{\circ}$

 $\theta = 30^{\circ}$

12

16 0

μ (meV)

- Y. A. Liao et al., Nature 467, 567-569 (2010).
- A. Hamo et al., Nature 535, 395-400 (2016).
- 8. G. Cheng et al., Nature 521, 196-199 (2015).
- A. Annadi et al., Nano Lett. 18, 4473-4481 (2018). 10. A. Rapp, G. Zaránd, C. Honerkamp, W. Hofstetter, Phys. Rev. Lett. 98. 160405 (2007).
- 11. T. Kraemer et al., Nature 440, 315-318 (2006).
- 12. R. Landauer, IBM J. Res. Develop. 1, 223-231 (1957)
- 13. D. L. Maslov, M. Stone, Phys. Rev. B 52, R5539-R5542 (1995).
- 14. S. Datta, Quantum Transport: Atom to Transistor (Cambridge Univ. Press, 2013).
- 15. B. J. van Wees et al., Phys. Rev. Lett. 60, 848-850 (1988).
- 16. D. A. Wharam et al., J. Phys. C 21, L209-L214 (1988).
- 17. A. Yacoby et al., Phys. Rev. Lett. 77, 4612-4615 (1996).
- 18. S. Frank, P. Poncharal, Z. L. Wang, W. A. Heer, Science 280, 1744-1746 (1998).
- 19. I. van Weperen, S. R. Plissard, E. P. A. M. Bakkers, S. M. Frolov, L. P. Kouwenhoven, Nano Lett. 13, 387-391 (2013).
- 20. G. Cheng et al., Phys. Rev. X 6, 041042 (2016).
- 21. See supplementary materials.
- 22. U. Schollwöck, Ann. Phys. 326, 96-192 (2011).
- 23. U. Schollwöck, Rev. Mod. Phys. 77, 259-315 (2005).
- 24. I. P. McCulloch, J. Stat. Mech. 2007, P10014 (2007).
- 25. I. P. McCulloch, arXiv 0804.2509 [cond-mat.str-el] (16 April 2008)
- 26. G. M. Crosswhite, A. C. Doherty, G. Vidal, Phys. Rev. B 78, 035116 (2008).
- 27. J. A. Kjäll, M. P. Zaletel, R. S. K. Mong, J. H. Bardarson,
- F. Pollmann, Phys. Rev. B 87, 235106 (2013).
- 28. P. W. Anderson, Phys. Rev. Lett. 34, 953-955 (1975). 29. R. de-Picciotto et al., Nature 389, 162-164 (1997).
- 30. L. P. Kouwenhoven, D. G. Austing, S. Tarucha, Rep. Prog. Phys. 64, 701-736 (2001)
- 31. C. S. O'Hern, T. C. Lubensky, J. Toner, Phys. Rev. Lett. 83, 2745-2748 (1999).
- 32. D. Pekker, G. Refael, E. Demler, Phys. Rev. Lett. 105, 085302 (2010).
- 33. P. Mohan, P. M. Goldbart, R. Narayanan, J. Toner, T. Vojta, Phys. Rev. Lett. 105, 085301 (2010).

34. C. L. Kane, A. Stern, B. I. Halperin, Phys. Rev. X 7, 031009 (2017).

8

B (T)

 $\theta = 50^{\circ}$

12 16

- 35. M. Briggeman, Pascal conductance series in ballistic onedimensional LAO/STO channels. Harvard Dataverse (2019); https://doi.org/10.7910/DVN/IXIFFX.
- 36. D. Pekker, Tri-GY. Harvard Dataverse (2019); https://doi.org/ 10.7910/DVN/ZZLDOX.

ACKNOWLEDGMENTS

 $\theta = 40^{\circ}$

16 0

12

8

B (T)

C

20 30 40 50

 θ (°)

60

dG/dμ (S/eV)

0.5

10

Funding: Supported by Vannevar Bush Faculty Fellowship ONR grant N00014-15-1-2847 and U.S. Department of Energy (DOE) Office of Science, Office of Basic Energy Sciences grant DE-SC0014417 (J.L., P.I.); NSF grants DMR-1609519 (J.L.), PHY-1913034 (J.L., D.P., and P.I.) and PIRE-1743717 (D.P.); and the Charles E. Kaufman Foundation (D.P.). Work at the University of Wisconsin-Madison (thin film synthesis and structural characterization) was supported by the U.S. Department of Energy (DOE), Office of Science, Basic Energy Sciences (BES) under award DE-FG02-06ER46327 (C.-B.E.). Author contributions: M.B.. M.T., and P.I. performed the experiments, analyzed data, and wrote the manuscript; B.T., Y.H., D.P., and R.S.K.M. performed the DMRG calculations and wrote the manuscript; A.T.-T. performed the single-particle model calculations and contributed to the manuscript writing: H.L., J.-W.L., and C.-B.E. grew and characterized the samples; M.H. processed the samples and patterned the interface electrodes; and J.L. directed the research, analyzed data, and wrote the manuscript. Competing interests: The authors declare no competing interests. Data and materials availability: Experimental datasets (35) and DMRG code (36) are available online at the Harvard Dataverse.

SUPPLEMENTARY MATERIALS

science.sciencemag.org/content/367/6479/769/suppl/DC1 Materials and Methods

Supplementary Text

Figs. S1 to S14

Table S1

Movie S1

References (37-46)

22 March 2018; resubmitted 23 October 2018 Accepted 14 January 2020 10.1126/science.aat6467



Pascal conductance series in ballistic one-dimensional LaAlO₃/SrTiO₃ channels

Megan Briggeman, Michelle Tomczyk, Binbin Tian, Hyungwoo Lee, Jung-Woo Lee, Yuchi He, Anthony Tylan-Tyler, Mengchen Huang, Chang-Beom Eom, David Pekker, Roger S. K. Mong, Patrick Irvin and Jeremy Levy

Science **367** (6479), 769-772. DOI: 10.1126/science.aat6467

An unusual conductance sequence

Effects of correlations between electrons are enhanced in systems of reduced dimensions. The two-dimensional interface between two oxide materials, lanthanum aluminate (LaAlO 3) and strontium titanate (SrTiO3), exhibits magnetism and superconductivity. In even lower-dimensional systems fabricated in similar heterostructures, electrons can pair without going superconducting. Briggeman *et al.* have now observed another exotic effect in LaAlO3/SrTiO3 waveguides: At certain magnetic fields, the conductance in these one-dimensional systems exhibits steps of an unconventional sequence. To understand the experimental data, the researchers used a model that accounted for interactions between electrons and found that the phenomenology was consistent with the formation of a series of correlated phases characterized by bound states of three or more electrons.

Science, this issue p. 769

ARTICLE TOOLS http://science.sciencemag.org/content/367/6479/769

SUPPLEMENTARY http://science.sciencemag.org/content/suppl/2020/02/12/367.6479.769.DC1 MATERIALS

REFERENCES This article cites 43 articles, 2 of which you can access for free

http://science.sciencemag.org/content/367/6479/769#BIBL

PERMISSIONS http://www.sciencemag.org/help/reprints-and-permissions

Use of this article is subject to the Terms of Service